ACS APPLIED MATERIALS & INTERFACES
Research Article
www.acsami.org

Tailoring the Valence Band Offset of Al_2O_3 on Epitaxial $GaAs_{1-y}Sb_y$ with Tunable Antimony Composition

Jheng-Sin Liu, Michael Clavel, and Mantu K. Hudait*

Advanced Devices & Sustainable Energy Laboratory (ADSEL), Bradley Department of Electrical and Computer Engineering, Virginia Tech, Blacksburg, Virginia 24061, United States

ABSTRACT: Mixed-anion, $GaAs_{1-y}Sb_y$ metamorphic materials with tunable antimony (Sb) compositions extending from 0 to 100%, grown by solid source molecular beam epitaxy (MBE), were used to investigate the evolution of interfacial chemistry under different passivation conditions. X-ray photoelectron spectroscopy (XPS) was used to determine the change in chemical state progression as a function of surface preclean and passivation, as well as the valence band offsets, conduction band offsets, energy band parameters, and bandgap of atomic layer deposited Al_2O_3 on $GaAs_{1-y}Sb_y$ for the first time, which is further corroborated by X-ray analysis and cross-sectional transmission electron microscopy. Detailed XPS analysis revealed that the near midpoint composition, $GaAs_{0.45}Sb_{0.55}$, passivation scheme exhibits a GaAs-like surface, and that precleaning by HCl and $(NH_4)_2S$ passivation are mandatory to remove native oxides from the surface of GaAsSb. The valence band offsets, ΔE_v, were determined from the difference in the core level to the valence band maximum binding energy of $GaAs_{1-y}Sb_y$. A valence band offset of >2 eV for all Sb compositions was found, indicating the potential of utilizing Al_2O_3 on $GaAs_{1-y}Sb_y$ ($0 \leq y \leq 1$) for p-type metal-oxide-semiconductor (MOS) applications. Moreover, Al_2O_3 showed conduction band offset of ~2 eV on $GaAs_{1-y}Sb_y$ ($0 \leq y \leq 1$), suggesting Al_2O_3 dielectric can also be used for *n*-type MOS applications. The surface passivation of $GaAs_{0.45}Sb_{0.55}$ materials and the detailed band alignment analysis of Al_2O_3 high-κ dielectrics on tunable Sb composition, $GaAs_{1-y}Sb_y$ materials, provides a pathway to utilize GaAsSb materials in future microelectronic and optoelectronic applications.

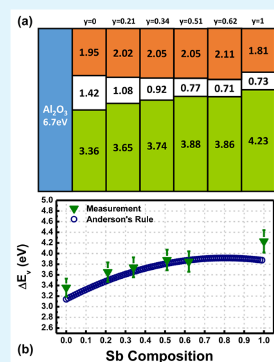

KEYWORDS: *broken gap, band alignments, GaAs/Al2O3, GaAsSb/Al2O3, GaAs/Al2O3, GaAsSb, epitaxy, molecular beam epitaxy, heterostructure*

INTRODUCTION

Arsenide−antimonide (As−Sb)-based material systems have been extensively investigated over several decades for mid-infrared optoelectronics and night vision imaging, as well as high-speed and ultralow power devices.[1,2] Specifically, Sb-based compound semiconductors (e.g., GaSb, AlSb, InSb) have been used in p-channel quantum well field effect transistor architectures, metal-oxide-semiconductor field effect transistors, and heterojunction tunnel field effect transistors (TFETs).[3,4] Recently, mixed-anion based $GaAs_{1-y}Sb_y$ materials are being considered as one of the most promising candidates for a widespread of device applications ranging from electronics to photonics.[5−8] The variable Sb composition in GaAsSb materials makes the system attractive for tunable bandgap lasers,[9−11] absorption in different wavelength regions of the solar spectrum,[12,13] and infrared photodetectors[14,15] applications. Furthermore, mixed As−Sb based $In_xGa_{1-x}As/GaAs_{1-y}Sb_y$ *n*-channel TFETs with adjustable band alignments, effective tunnel barrier height (E_{beff}), and bandgaps were achieved by varying Sb alloy composition in GaAsSb, which is internally lattice matched with InGaAs for a given alloy composition of Sb and indium (In).[16] However, for a complementary *p*-channel TFETs, $GaAs_{1-y}Sb_y$ material was used to serve as a channel material in GaAsSb/InGaAs TFETs configuration. In this case, integration of a superior high-κ gate dielectric on the GaAsSb material system for any Sb composition remains elusive to date due to the formation of complex native oxides on the GaAsSb surface.[17] Thus, there is a major challenge in achieving a low interface density at the high-κ gate dielectric/GaAsSb heterointerface that necessitates the surface passivation of $GaAs_{1-y}Sb_y$ dangling bonds for tunable Sb compositions ($0 \leq y \leq 1$). Besides, there are many fundamental challenges that arise in attempting to achieve device-quality, compositional dependent $GaAs_{1-y}Sb_y$ materials due to the different surface sticking coefficients of Sb_2 and As_2 species during growth. First and foremost, there is a challenge to control the defects in GaAsSb materials with higher Sb composition integrated on GaAs substrates using metamorphic graded buffers due to the large lattice mismatch between the film and the substrate. Second, there is a challenge to demonstrate tunable Sb compositions with well-controlled defects in the GaAsSb materials during epitaxy. Third, the removal of native oxide with wet chemical processes that simultaneously remove complex native oxides[18−20] and passivate the GaAsSb surface prior to deposition of high-κ dielectric layer.

Received: October 24, 2015
Accepted: December 7, 2015

ACS Publications © XXXX American Chemical Society

DOI: 10.1021/acsami.5b10176
ACS Appl. Mater. Interfaces XXXX, XXX, XXX−XXX

In the past, Al_2O_3 high-κ dielectric was used on GaAs and GaSb materials using atomic layer deposition (ALD) for transistor applications.[21−23] Unlike SiO_2 grown on Si, the native oxide of $GaAs_{1-y}Sb_y$ is a complex mixture of GaO_x, AsO_x, and SbO_x, as investigated by several researchers.[17,24−27] Developing a proper technique for the replacement of native oxide and passivation of oxide-semiconductor interface would make it possible to achieve a precise band alignment determination of Al_2O_3 on Sb compositionally dependent $GaAs_{1-y}Sb_y$. Although, sulfur (S) passivation and the band alignment of either Al_2O_3/GaAs or Al_2O_3/GaSb were reported,[28,29] the surface passivation and the energy band alignment of Al_2O_3 on $GaAs_{1-y}Sb_y$ with tunable Sb composition is sparse and remains unknown. This study focuses on the properties of sulfur passivated GaAsSb surfaces with higher Sb compositions as well as Sb compositional dependent valence band and conduction band offsets of $Al_2O_3/GaAs_{1-y}Sb_y$ interfaces. The Sb and As composition in GaAsSb materials were determined by X-ray diffraction (XRD) measurement. X-ray photoelectron spectroscopy (XPS) measurements were carried out to determine the band alignment at the $Al_2O_3/GaAs_{1-y}Sb_y$ interface for varying Sb compositions. Moreover, cross-sectional transmission electron microscopy (TEM) measurements were performed to investigate the defect and structural properties of selected GaAsSb samples. The compositional dependent band alignment and detailed surface passivation schemes on the $GaAs_{1-y}Sb_y$ films are a significant step toward the development of $In_xGa_{1-x}As/GaAs_{1-y}Sb_y$-based transistor and multifunctional device applications.

RESULTS AND DISCUSSION

Material Characterization. *X-ray Analysis.* Figure 1a shows the X-ray rocking curve of the $GaAs_{0.66}Sb_{0.34}$ sample grown on (100)/2° GaAs using a 2-step metamorphic graded buffer. The step-graded buffer was used to mitigate lattice mismatch induced defects and dislocations. The peak position of the targeted GaAsSb composition is located on the left side of the GaAs substrate indicating a larger lattice constant material. The Sb composition of each layer structure is indicated in Figure 1a. The layer compositions and the relaxation states were determined utilizing X-ray reciprocal space maps (RSMs). The symmetric (004) and asymmetric (115) RSMs shown in Figure 1b,c, were recorded to determine the perpendicular and parallel lattice constants of each layer and hence the layer composition and the degree of relaxation.[30] The out-of-plane lattice constant, c (taken from the symmetric 004 reflection) and the lattice constant in the growth plane, a (taken from the asymmetric 115 reflection) were determined from the measured RSMs. The relaxed lattice constant, a_r, and strain relaxation values were extracted from each RSM using the methods introduced in refs 30−32. The determination of strain relaxation values was performed as a sequence from the bottom layer to the top layer, and all relaxation values were determined with respect to the GaAs substrate. The uppermost composition of the $GaAs_{0.66}Sb_{0.34}$ layer of interest was ~90% relaxed. One can also find in Figure 1b that the reciprocal lattice point (RLP) for each layer was not aligned vertically with the substrate RLP, indicating a minor amount of lattice tilt with respect to the substrate. From Figure 1a, the values of tilts were determined to be −816, −562, and −430 arcsec for $GaAs_{0.85}Sb_{0.15}$, $GaAs_{0.76}Sb_{0.24}$, and $GaAs_{0.66}Sb_{0.34}$, respectively. The detailed X-ray analysis of additional Sb compositions were reported elsewhere.[32] The X-ray analysis of the $GaAs_{0.49}Sb_{0.51}$ sample was further corroborated by cross-sectional TEM measurement and analysis below to gain further insight into the defect properties and structural quality of the mixed-anion $GaAs_{1-y}Sb_y$ material system.

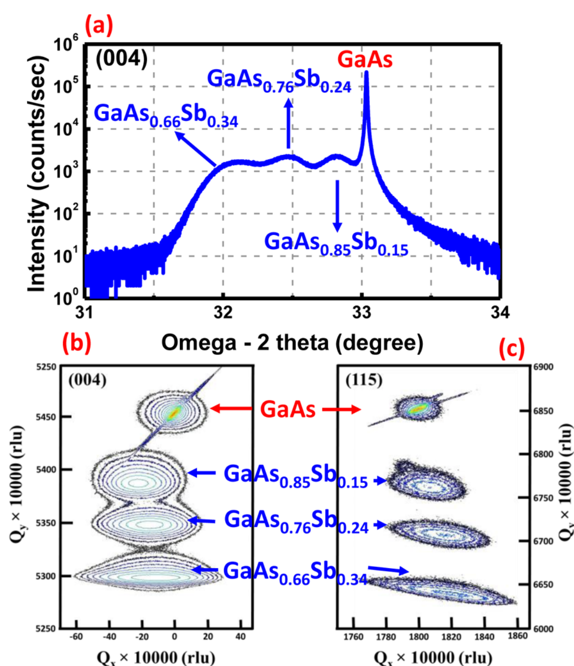

Figure 1. (a) X-ray rocking curve and (b) symmetric and (c) asymmetric reciprocal space maps of $GaAs_{0.66}Sb_{0.34}$ layer grown (100)/2° GaAs substrate using two-step graded buffer.

TEM Analysis. Cross-sectional TEM micrographs were taken from a $GaAs_{1-y}Sb_y$ sample having 51% Sb composition, shown in Figure 2a. As shown in Figure 2a, a large fraction of misfit-induced defects resulting from the lattice mismatch between the first Sb composition layer, $GaAs_{0.51}Sb_{0.49}$ and the GaAs substrate, were confined within a thickness of about 0.5 μm. One can also find from Figure 2a that sharp heterointerfaces were observed at each $GaAs_{1-y}Sb_y$ interface, labeled as L1 and L2 in Figure 2b, which is essential in minimizing the interface and surface-related charge carrier scattering in the $GaAs_{1-y}Sb_y$ active layer and for the integration of high-κ dielectrics for multifunctional device applications.

Figure 2c shows the high-resolution cross-sectional TEM micrograph of the $Pt/Al_2O_3/GaAs_{0.49}Sb_{0.51}$ MOS structure. The relative uniformity of the $Al_2O_3/GaAs_{0.49}Sb_{0.51}$ interface is clearly visible in the high-resolution TEM micrograph. This micrograph also demonstrates the abrupt nature of the heterointerface. Further, the TEM results demonstrate the high degree of coherency of the ALD deposited 6.8 nm thick amorphous Al_2O_3 layer on $GaAs_{0.49}Sb_{0.51}$ layer. The observed uniformity at the interface between the amorphous Al_2O_3 and the $GaAs_{0.49}Sb_{0.51}$ layer is indispensable in minimizing interface scattering for carrier transport in future GaAsSb based MOS devices. Utilizing this $Al_2O_3/GaAs_{0.49}Sb_{0.51}$ heterointerface, one can achieve superior transport characteristics such as lower interface states, reduced frequency dispersion, lower capacitance−voltage hysteresis, and targeted equivalent oxide layer thickness, all needed for ultralow power tunnel transistors based on GaAsSb/InGaAs system.

XPS Analysis. *Surface Passivation.* The Sb compositional dependent valence band and conductance band offsets of

DOI: 10.1021/acsami.5b10176
ACS Appl. Mater. Interfaces XXXX, XXX, XXX−XXX

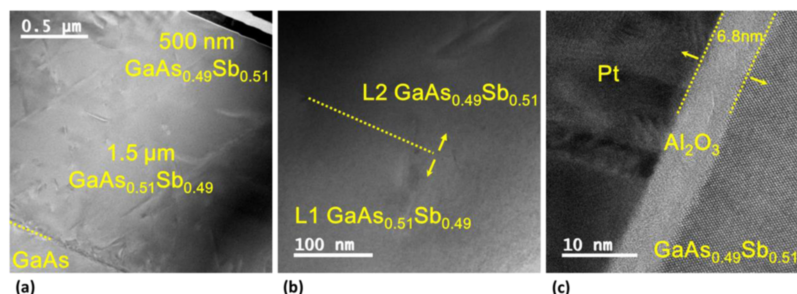

Figure 2. (a) Cross-sectional TEM micrograph of $GaAs_{0.49}As_{0.51}$ grown on a (100)/2° GaAs substrate using metamorphic graded $GaAs_{1-y}Sb_y$ buffer layer. The boundary of two are difficult to define because of low magnification. (b) The Sb composition of the uppermost GaAsSb layer is close to that of the two-step metamorphic graded buffer layers, where metamorphic buffer layers L1 and L2 also exhibited similar Sb compositions relative to each other; yellow dashed line shows two GaAsSb layers of close Sb compositions (49% Sb and 51% Sb). (c) High-resolution TEM micrograph of the $Pt/Al_2O_3/GaAs_{0.49}As_{0.51}$ interface, demonstrating a sharp heterointerface between Al_2O_3 and $GaAs_{0.49}As_{0.51}$.

GaAsSb with high-κ dielectrics, such as Al_2O_3, has great significance for tunable tunnel barrier height InGaAs/GaAsSb based heterojunction TFETs. The formation of complex native oxides on the GaAsSb surface (i.e., Sb_2O_3, As_2O_3, Ga_2O_3, etc.)[25,33] makes the GaAsSb material system difficult to control the interface defect density especially for p-channel TFETs application. Various wet chemical processes to passivate the surface of either GaAs or GaSb materials have been prescribed by several studies.[27−29,34,35] However, the surface passivation study on the GaAsSb material system is unclear or remains unknown. Here, we have systematically studied the surface passivation schemes of $GaAs_{0.45}Sb_{0.55}$ layers by XPS. This Sb composition was selected since it is almost the midpoint composition of the GaAs-GaSb material system. Different combinations of cleaning processes were developed and implemented on the selected composition of epitaxial $GaAs_{0.45}Sb_{0.55}$, GaAs, and GaSb surfaces for this study. In this particular work, four samples were selected to investigate the effect of preclean and surface passivation prior to the deposition of Al_2O_3 layer on $GaAs_{0.45}Sb_{0.55}$: (1) as-received $GaAs_{0.45}Sb_{0.55}$ layer, (2) HCl-treated $GaAs_{0.45}Sb_{0.55}$ epi-layer, (3) $(NH_4)_2S$-treated $GaAs_{0.45}Sb_{0.55}$ epi-layer, and (4) HCl plus $(NH_4)_2S$-treated $GaAs_{0.45}Sb_{0.55}$ epi-layer.

Figure 3 shows the Ga 3d and O 2s as well as As 3d and Sb 4d spectra recorded from the surface of each sample, respectively. The peak positions of each sample were shifted as well as aligned vertically to observe the peak evolution due to the surface cleaning and passivation methods. The Ga−O (21.0 eV), As−O (44.7 eV), and Sb−O (34.2 eV) peaks were found from the as-grown $GaAs_{0.45}Sb_{0.55}$ layer, as expected, due to the lack of surface precleaning prior to the XPS measurement. The as-grown $GaAs_{0.45}Sb_{0.55}$ sample was precleaned using HCl and the subsequent XPS measurement demonstrated minimal amount of Ga−O and As−O peaks, as shown in Figure 3, indicating the effectiveness of HCl to remove the native oxides of Ga−O and As−O from the surface of $GaAs_{0.45}Sb_{0.55}$. On the other hand, the HCl has limited effect for the removal of the Sb−O native oxide peak. The as-grown $GaAs_{0.45}Sb_{0.55}$ sample was then passivated using $(NH_4)_2S$ without precleaning by HCl and the corresponding peaks are also shown in Figure 3. One can find that the native oxides (i.e., a mixture of Ga−O, As−O, and Sb−O) were effectively removed from the surface of as-grown $GaAs_{0.45}Sb_{0.55}$ by $(NH_4)_2S$. Furthermore, the Ga−O and Sb−O peaks unable to be removed by HCl were successfully removed by $(NH_4)_2S$ passivation. It is interesting to note that the Ga and Sb remain bound to S via $(NH_4)_2S$ processing even after a 30 min window between the initial passivation and when the samples were loaded and the XPS spectra recorded. This indicates that the Ga−S and Sb−S bonds are stable for at least 30 min in atmosphere, which is important where a long pause between the surface passivation and the deposition of high-κ dielectric could not be avoided. Finally, the as-grown $GaAs_{0.45}Sb_{0.55}$ sample was precleaned by HCl and subsequently passivated using $(NH_4)_2S$ and the corresponding XPS spectra are shown in Figure 3. As shown in Figure 3, the Ga and Sb were bound to S and the As−O peak was eliminated by this combined wet chemical process. Therefore, one can conclude that either $(NH_4)_2S$ or the combination of HCl and $(NH_4)_2S$ processes on mixed As−Sb based GaAsSb materials are essential to clean and passivate the surface prior to the deposition of high-κ dielectrics.

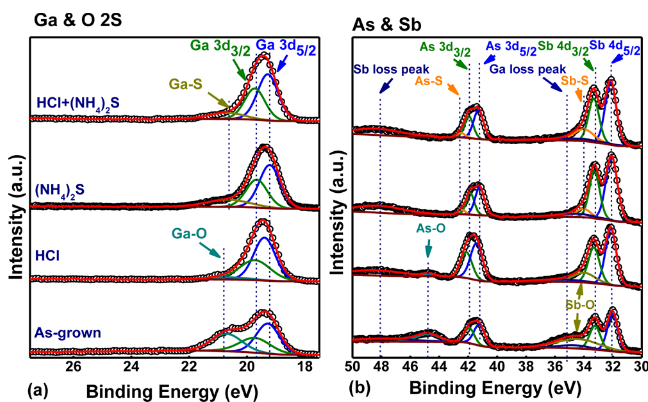

Figure 3. (a) Ga 3d and O 2s and (b) As 3d and Sb 4d XPS spectra, showing the chemical state evolution as a function of surface preclean and passivation on $GaAs_{0.45}Sb_{0.55}$. The peak positions of each sample were shifted and aligned vertically to observe the peak development due to the surface cleaning and passivation.

ALD Al_2O_3 (1.5 nm) with HCl and $(NH_4)_2S$ Surface Passivation of GaAs and GaSb Surfaces. The combined HCl and $(NH_4)_2S$ scheme was used to passivate the $GaAs_{0.45}Sb_{0.55}$ sample prior to the deposition of Al_2O_3. Besides passivated $GaAs_{0.45}Sb_{0.55}$, an as-grown $GaAs_{0.45}Sb_{0.55}$ sample was used along with GaAs and GaSb samples. The GaAs and GaSb samples were cleaned and passivated (HCl and $(NH_4)_2S$), and placed in the ALD chamber for the deposition of the 1.5 nm Al_2O_3 layer. The combination of an HCl preclean, sulfur passivation and ALD deposited 1.5 nm Al_2O_3 were considered as a prescribed solution for the removal of native oxides on GaAs and GaSb samples.[36,19] Here, we have

DOI: 10.1021/acsami.5b10176
ACS Appl. Mater. Interfaces XXXX, XXX, XXX−XXX

utilized these steps on the GaAs and GaSb samples to observe the effect of passivation. All four samples (as-grown $GaAs_{0.45}Sb_{0.55}$, passivated $GaAs_{0.45}Sb_{0.55}$, GaAs and GaSb) were loaded together into the XPS chamber for measurement.

Figure 4 shows the Ga 3d and O 2s, as well as As 3d and Sb 4d, spectra recorded from the surface of each sample for different passivation conditions, respectively. In these figures, peak positions of each sample were shifted vertically to make all binding energies for of main element are aligned to the same position. From the XPS spectrum of GaAs and GaSb samples shown in Figure 4b, the As−O (44.7 eV) and Sb−O (34.2 eV) bond peaks were eliminated due to the combined effect of preclean, sulfur passivation, and ALD deposited Al_2O_3 layer by trimethylaluminum (TMA) precursor.[27,34] It has been reported that the self-cleaning mechanism requires lower Gibbs free energy of material.[34] Indeed, the Al_2O_3 material has lower Gibbs free energy (−377.9 kcal/mol) than the energies of native oxides, which are Ga_2O, Ga_2O_3, As_2O_3, As_2O_5, and Sb_2O_3 (−75.3, −238.6, −137.7, −187.0, and −151.5 kcal/mol, respectively).[25,37] Therefore, the Al_2O_3 layer is more stable during the formation of Al_2O_3 oxide by ALD, and further, it assisted in the removal of surface native oxides.[34] The TMA used in ALD for the Al_2O_3 deposition has an energetic preference to the native oxides on GaAs. In this case, the Gibbs free energy of As−O bonds were higher than Ga−O bonds, indicating that Ga−O bonds were more stable than As−O bonds during Al_2O_3 deposition, which has been shown in Figure 4a. The peak position of the Ga−O bond (∼21 eV) in the GaAs sample after sulfur passivation and Al_2O_3 layer deposition, is replaced by the presence of the Ga−S bond (dark orange color), indicating the strong surface passivation of the GaAs layer with the combined effect of preclean, sulfur passivation and Al_2O_3 layer deposition. On the other hand, the mixture of Ga−S and Ga−O bond peaks both at ∼21 eV were observed from the GaSb sample, where the integrated peak area (orange color) with respect to the background is significantly higher than on the GaAs sample with the same cleaning process, exhibiting the less pronounced passivation as well as self-cleaning effect on the GaSb sample. Due to the presence of the Ga−O (or Ga−S) peak at ∼21 eV (which is difficult to decouple due to the similar binding energies of Ga−O and Ga−S)[34] even after sulfur passivation and Al_2O_3 deposition, one can find it difficul to achieve superior quality metal-oxide-semiconductor (MOS) capacitor characteristics for future low power electronic devices. Thus, the surface passivation of the GaSb is more challenging than the GaAs under the same HCl preclean and sulfur passivation conditions. It is interesting to investigate the detailed surface passivation of the mixed $GaAs_{0.45}Sb_{0.55}$ sample with different passivation conditions and the self-cleaning (if any) by Al_2O_3 deposition. This passivation study will provide information as to whether this material would exhibit either GaAs-like or GaSb-like passivation behavior because it is not well-understood in the literature.

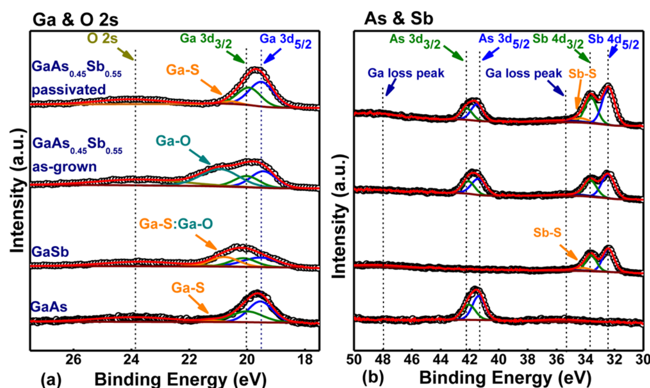

Figure 4. (a) Ga 3d and O 2s and (b) As 3d and Sb 4d XPS spectra, respectively, showing the existence of bonds as a function of surface preclean, passivation, and atomic layer deposited Al_2O_3. Peak positions of each sample were shifted vertically to align main element binding energies to the same position. The Ga−O peak from the as-grown $GaAs_{0.45}Sb_{0.55}$ with Al_2O_3, and the mixture of the Ga−O and Ga−S peaks from the GaSb sample after the HCl preclean, sulfur passivation and 1.5 nm Al_2O_3 layer shows the difficulty to make GaSb-based MOS devices. These peaks were eliminated from the GaAs and the $GaAs_{0.45}Sb_{0.55}$ layers after the HCl preclean, sulfur passivation and 1.5 nm Al_2O_3 layer, which can significantly affect the device performance.

ALD Al_2O_3 (1.5 nm) with HCl and $(NH_4)_2S$ Surface Passivation of GaAsSb Surface. Figure 4 also shows the Ga 3d and O 2s, as well as As 3d and Sb 4d, spectra, recorded from the surface of $GaAs_{0.45}Sb_{0.55}$ samples: (1) 1.5 nm Al_2O_3 on an as-grown sample and (2) 1.5 nm Al_2O_3 on the HCl precleaned and sulfur passivated sample. One can find from Figure 4a that the as-grown sample exhibits a strong Ga−O peak around 21 eV (cyan color), even after the atomic layer deposited 1.5 nm Al_2O_3, which indicates that the $GaAs_{0.45}Sb_{0.55}$ surface is not self-cleaned by TMA during the Al_2O_3 deposition. It is interesting to note that the Sb−O related peak (∼34.2 eV) was not observed from the as-grown sample after Al_2O_3 deposition. Also, the As−O related peak (∼44.7 eV) was not observed from the as-grown sample. These indicate that both As−O and Sb−O bonds can easily be removed during Al_2O_3 deposition from as-grown $GaAs_{0.45}Sb_{0.55}$ sample. The absence of As−O and Sb−O peaks from the surface of $GaAs_{0.45}Sb_{0.55}$ layer by ALD deposited Al_2O_3 is believed to be caused by the effect of the "self-cleaning" process observed for the first time to our knowledge. The measures must be taken to remove or passivate the Ga−O peak from the $GaAs_{0.45}Sb_{0.55}$ surface. The as-grown $GaAs_{0.45}Sb_{0.55}$ film was precleaned with HCl and passivated with sulfur prior to the deposition of 1.5 nm Al_2O_3 to investigate the effect of precleaning and sulfur passivation on the Ga−O bond. One can find from Figure 4a that the Ga−O peak which was observed in the as-grown sample, was eliminated by the above passivation scheme. The Ga−S and Sb−S peaks were observed around 20.5 and 34.2 eV, respectively. In the passivated $GaAs_{0.45}Sb_{0.55}$, the S passivation suppressed the formation of Ga−O bonds and contributed to Ga−S and Sb−S bonds, shown in Figure 4 (the existence of S 2s peak not shown here confirmed the S related bonds). The S atom replaced the surface positon of oxygen atoms that were previously bonded with Ga and Sb atoms, thus preventing the formation of GaO_x and SbO_x native oxides. The Ga−O peak from the as-grown $GaAs_{0.45}Sb_{0.55}$ with Al_2O_3, and the mixture of Ga−O and Ga−S peaks from GaSb sample after the HCl preclean, sulfur passivation and 1.5 nm Al_2O_3 layer, shows the difficulty to demonstrate GaSb-based MOS devices. These peaks were eliminated after the HCl preclean, sulfur passivation and 1.5 nm Al_2O_3 layer deposition. Therefore, the surface passivation effect on $GaAs_{0.45}Sb_{0.55}$ has a close resemblance with the GaAs surface, which is beneficial for the electrical transport characteristics of GaAsSb-based MOS devices.

Band Alignment. High-resolution XPS was performed to determine the valence band offset (ΔE_v) of Al_2O_3/ $GaAs_{1-y}Sb_y$ with tunable Sb composition ($0 \leq y \leq 1$). The band alignments

DOI: 10.1021/acsami.5b10176
ACS Appl. Mater. Interfaces XXXX, XXX, XXX−XXX

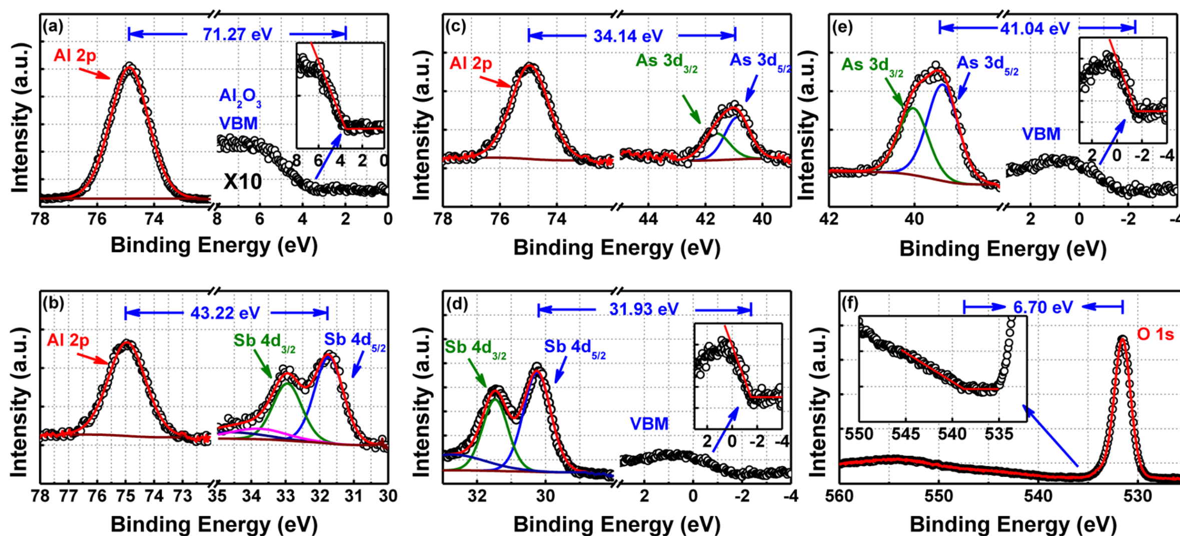

Figure 5. XPS spectra of (a) Al 2p from the 10 nm Al_2O_3, (b) from the interface of 1.5 nm Al_2O_3/ $GaAs_{0.49}Sb_{0.51}$ with Sb as a reference CL, (c) from the interface of 1.5 nm Al_2O_3/ $GaAs_{0.49}Sb_{0.51}$ with As as a reference CL, (d) Sb CL and valence band maximum, (e) As CL and valence band maximum, and (f) O 1s spectrum.

were determined by the energy difference between the core levels (CLs) and the valence band maxima (VBM) spectra recorded from each Al_2O_3 and $GaAs_{1-y}Sb_y$ surface. Kraut's method[38] was used to calculate ΔE_v by using the following equations:

$$\Delta E_{v,Sb} = (E_{Sb4d_{5/2}}^{GaAsSb} - E_{VBM}^{GaAsSb}) - (E_{Al2p}^{Al_2O_3} - E_{VBM}^{Al_2O_3}) - (E_{Sb4d_{5/2}}^{GaAsSb} - E_{Al2p}^{Al_2O_3})$$

$$\Delta E_{v,As} = (E_{As3d_{5/2}}^{GaAsSb} - E_{VBM}^{GaAsSb}) - (E_{Al2p}^{Al_2O_3} - E_{VBM}^{Al_2O_3}) - (E_{As3d_{5/2}}^{GaAsSb} - E_{Al2p}^{Al_2O_3}) \quad (1)$$

where, $\Delta Ev_{,Sb}$ and $\Delta Ev_{,As}$ are the valence band offset based on the VBM and CL of Sb and As, respectively. This will provide the difference in band offset value (if any) for a given Sb composition using either As or Sb CL spectrum. To determine the band offset, we recorded the following spectra: (1) the binding energy difference between the Sb $4d_{5/2}$ (As $3d_{5/2}$) CL and VBM of GaAsSb, $(E_{Sb\ 4d_{5/2}}^{GaAsSb} - E_{VBM}^{GaAsSb})$ $(E_{As\ 3d_{5/2}}^{GaAsSb} - E_{VBM}^{GaAsSb})$ from the bulk $GaAs_{1-y}Sb_y$ surface; (2) the binding energy difference between the Al 2p CL and the VBM of Al_2O_3, $(E_{Al\ 2p}^{Al_2O_3} - E_{VBM}^{Al_2O_3})$, from 10 nm thick Al_2O_3; and (3) the binding energy difference between the Al_2O_3 and Sb (As) $(E_{Sb\ 4d_{5/2}}^{GaAsSb} - E_{Al\ 2p}^{Al_2O_3})$ $(E_{As\ 3d_{5/2}}^{GaAsSb} - E_{Al\ 2p}^{Al_2O_3})$ CLs from the interface of 1.5 nm Al_2O_3/ $GaAs_{1-y}Sb_y$, respectively, and the results of such spectra are shown in Figure 5. As shown in Figure 4, the passivated sample showed the suppression of oxygen bonds and enhanced passivation of dangling bonds by sulfur. Since the Ga peak has a stronger coupling between Ga−O and Ga−S bonds and the Ga CL, the Sb and As CL peak references would allow for the independent confirmation of the band alignment results. Utilizing eq 1 and the measured XPS spectra, $\Delta E_{v,Sb}$ ($\Delta E_{v,As}$) for $GaAs_{1-y}Sb_y$ samples with tunable Sb compositions were determined. For the GaAs and GaSb samples, the corresponding spectra were recorded.

The band gap (E_g) value of ALD deposited Al_2O_3 for each Sb composition was determined by using the energy-loss peak of O 1s spectrum.[39,40] The binding energy was calculated from the difference in the total photoelectron energy minus the kinetic energy due to the loss in photoelectron energy by inelastic collision processes within the sample. The minimum inelastic loss is equal to the bandgap energy. The intersection of the linear extrapolation of the loss energy spectra and "zero level" shows the onset of inelastic losses. Thus, the bandgap energy is the energy difference between the O 1s peak and the onset of inelastic spectra. The results shown in Figure 5f for 10 nm ALD Al_2O_3 is approximately 6.70 eV. All parameters and energies acquired from XPS measurements are listed in Table 1.

On the basis of the experimental data of ΔE_v, E_g, and theoretical bandgap of $GaAs_{1-y}Sb_y$ (y = 0, 0.21, 0.34, 0.51, 1)[41] shaded white in Figure 6a, the conduction band offset, ΔE_c as a function of tunable Sb composition can be expressed as

$$\Delta E_c = E_{g,Al_2O_3} - E_{g,GaAsSb} - \Delta E_v \quad (2)$$

The band alignment parameters are summarized in Figure 6a and listed in Table 1. Figure 6a also visualizes the detailed band alignment parameters of $Al_2O_3/GaAs_{1-y}Sb_y$ for different Sb compositions. The electron affinity of GaAs and GaSb are 4.07 and 4.06 eV, respectively, so the electron affinities for different Sb compositions in GaAsSb are very similar. It implies that the major changes in band offset are contributed from the change in valence band as a function of Sb composition. It is interesting to note that the ΔE_v determined by both Sb and As CL spectra showed very similar results, shown in Table 1, thereby reinforcing the ΔE_v values for each As or Sb composition in $GaAs_{1-y}Sb_y$ acquired from XPS measurements. One can find that the ΔE_v and ΔE_c values are both larger than 2 eV for different Sb compositions. The higher band offset values are needed to suppress the leakage current between the dielectric and the GaAsSb channel material. The Anderson band alignment model[42] was used to validate the ΔE_v trend as a function of Sb composition. One can find that the Anderson band alignment model is in agreement with the measured ΔE_v values. There is a discrepancy between the model and the experimental results on GaSb compared with GaAsSb samples. In Anderson's model, the valence band offset between the Al_2O_3 and epitaxial GaAsSb materials are determined by considering (1) the electron affinity difference between those materials and (2) the bandgap of each GaAsSb. Both the measured XPS data and Anderson's model predicted very similar conduction band offset value for GaAsSb samples. However, the presence of native oxides on GaSb sample, even

DOI: 10.1021/acsami.5b10176
ACS Appl. Mater. Interfaces XXXX, XXX, XXX−XXX

Table 1. Binding Energy Difference

material and interface	binding energy difference	GaAs (eV)	$GaAs_{0.79}Sb_{0.21}$ (eV)	$GaAs_{0.66}Sb_{0.34}$ (eV)	$GaAs_{0.49}Sb_{0.51}$ (eV)	$GaAs_{0.38}Sb_{0.62}$ (eV)	GaSb (eV)
thick Al_2O_3 (10 nm)	$E^{Al_2O_3}_{Al\ 2p} - E^{Al_2O_3}_{VBM}$	71.28	71.20	71.13	71.27	71.10	71.04
interface (1.5 nm Al_2O_3 on GaAsSb, using Sb peak)	$E^{GaAsSb}_{Sb\ 4d_{5/2}} - E^{Al_2O_3}_{Al\ 2p}$	N.A.	−43.20	−43.16	−43.22	−43.17	−42.90
interface (1.5 nm Al_2O_3 on GaAsSb, using As peak)	$E^{GaAsSb}_{As\ 3d_{5/2}} - E^{Al_2O_3}_{Al\ 2p}$	−33.72	−34.06	−34.07	−34.14	−34.07	N.A.
thick GaAsSb (epitaxy, using Sb peak)	$E^{GaAsSb}_{Sb\ 4d_{5/2}} - E^{GaAsSb}_{VBM}$	N.A.	31.66	31.71	31.93	31.78	32.37
thick GaAsSb (epitaxy, using As peak)	$E^{GaAsSb}_{As\ 3d_{5/2}} - E^{GaAsSb}_{VBM}$	40.92	40.73	40.74	41.04	40.91	N.A.
E_g (Al_2O_3)	from this work	6.74	6.75	6.71	6.70	6.69	6.71
E_g (GaAsSb)	$1.2y^2 - 1.9y + 1.43$, y = Sb composition	1.42	1.08	0.92	0.77	0.71	0.73
$\Delta E_v = (E^{Al_2O_3}_{VBM} - E^{GaAsSb}_{VBM})$ (estimated by Sb peak)	$(E^{GaAsSb}_{Sb\ 4d_{5/2}} - E^{GaAsSb}_{VBM}) - (E^{Al_2O_3}_{Al\ 2p} - E^{Al_2O_3}_{VBM}) - (E^{GaAsSb}_{Sb\ 4d_{5/2}} - E^{Al_2O_3}_{Al\ 2p})$	N.A.	3.65	3.74	3.88	3.86	4.23
$\Delta E_v = (E^{Al_2O_3}_{VBM} - E^{GaAsSb}_{VBM})$ (estimated by As peak)	$(E^{GaAsSb}_{As\ 3d_{5/2}} - E^{GaAsSb}_{VBM}) - (E^{Al_2O_3}_{Al\ 2p} - E^{Al_2O_3}_{VBM}) - (E^{GaAsSb}_{As\ 3d_{5/2}} - E^{Al_2O_3}_{Al\ 2p})$	3.36	3.59	3.69	3.91	3.88	N.A.
ΔE_C (estimated by Sb peak)	$E^{Al_2O_3}_g - E^{GaAsSb}_g - \Delta E_v$	N.A.	2.02	2.05	2.05	2.11	1.75
ΔE_C (estimated by As peak)	$E^{Al_2O_3}_g - E^{GaAsSb}_g - \Delta E_v$	1.95	2.08	2.10	2.02	2.09	N.A.

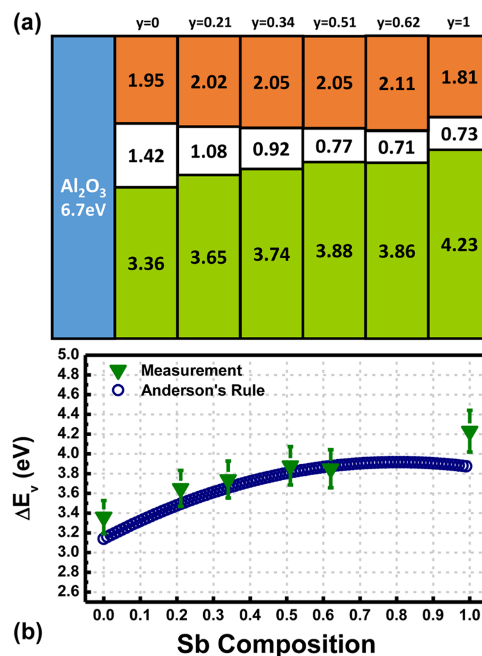

Figure 6. (a) Energy band parameters for A_2O_3 on $GaAs_{1-y}Sby$ with tunable Sb composition and (b) the measured valence band offset as a function of Sb composition along with the modeled band alignment results obtained using Anderson's rule.

after sulfur passivation and Al_2O_3 layer deposition, affects the valence band offset and the resulting conduction band offset due to the differences in GaSb bandgap and the measured valence band offset. Thus, we believe that due to difficulty in cleaning and passivation of GaSb surface, there is a difference in conduction band offset between Al_2O_3 and GaSb sample. Combining the benefits of the nature of the band alignments between GaAsSb/InGaAs and the higher energy barrier of Al_2O_3/GaAsSb, Al_2O_3 has been found to be a promising high-κ gate dielectric on mixed As−Sb based GaAsSb materials.

CONCLUSIONS

$GaAs_{1-y}Sb_y$ ($0 \le y \le 1$) metamorphic materials with tunable Sb compositions grown by solid source MBE were used to investigate the evolution of interfacial chemistry under different passivation conditions. X-ray photoelectron spectroscopy was used to determine the chemical state evolution as a function of surface preclean and passivation, as well as valence band and conduction band offsets, energy band parameters, and bandgap of atomic layer deposited Al_2O_3 on $GaAs_{1-y}Sb_y$ for the first time, which is further corroborated by X-ray analysis and cross-sectional TEM. Detailed XPS analysis revealed that the near midpoint composition $GaAs_{0.45}Sb_{0.55}$ passivation scheme exhibits a GaAs-like surface and that precleaning by HCl and $(NH_4)_2S$ passivation are mandatory to remove the native oxides from the surface of GaAsSb. A valence band offset >2 eV for all Sb compositions indicates the potential of utilizing Al_2O_3 on $GaAs_{1-y}Sb_y$ ($0 \le y \le 1$) for *p*-type metal-oxide-semiconductor device applications. Moreover, Al_2O_3 showed a conduction band offset of ~2 eV on $GaAs_{1-y}Sb_y$, suggesting Al_2O_3 dielectric can also be used for *n*-type MOS device applications. Therefore, the surface passivation and the detailed band alignment analysis of Al_2O_3 on tunable Sb composition, $GaAs_{1-y}Sb_y$, provides a pathway to utilize $GaAs_{1-y}Sb_y$ materials in multifunctional device applications.

DOI: 10.1021/acsami.5b10176
ACS Appl. Mater. Interfaces XXXX, XXX, XXX−XXX

MATERIALS AND METHODS

Material Synthesis. The $GaAs_{1-y}Sb_y$ layers with tunable Sb composition were grown by solid source MBE on semi-insulating (100)/2° GaAs substrates. The Sb flux was provided by a low-temperature 125 cm^3 Sb effusion cell and arsenic valved cracker source for As_2 flux with the cracking zone held at 900 °C. Substrate oxide desorption was performed at ~735 °C thermocouple temperature under a constant As_2 flux and the surface was monitored by in situ reflected high energy electron diffraction. A 0.5 μm/h growth rate was used for all GaAsSb samples. For each structure, several layers of $GaAs_{1-y}Sb_y$ were grown using different As/Ga (5−15) and Sb/Ga (1−6.16) ratios as well as different substrate temperatures (375−450 °C) so as to yield a tunable Sb composition.[43] To achieve the higher Sb composition, we used a higher Sb/Ga ratio and lower growth temperature during growth. Besides, to accommodate the lattice mismatch between the top $GaAs_{1-y}Sb_y$ layer of interest and the GaAs substrate as well as to reduce the threading dislocation density in the final $GaAs_{1-y}Sb_y$ layer, a two-step graded GaAsSb layer with different Sb compositions was incorporated in each run. The thickness of each layer was fixed at 750 nm. The growth parameters used for the different $GaAs_{1-y}Sb_y$ layers and the detailed X-ray analysis were reported earlier.[32]

Materials Characterization. The alloy composition and strain relaxation properties of $GaAs_{1-y}Sb_y$ layer were characterized by high-resolution XRD. Both the X-ray rocking curve ($\omega/2\theta$ scan) and the reciprocal space maps for each sample were obtained using a Panalytical X'pert Pro system with Cu Kα-1 as the X-ray source. The interface quality between the atomic layer deposited Al_2O_3 and the GaAsSb layer, as well as the defect properties of the GaAsSb, were examined using high-resolution TEM analysis performed on a JEOL 2100 microscope. The electron-transparent foils of thin-film cross-section of $Al_2O_3/GaAs_{0.49}Sb_{0.51}/GaAs_{1-y}Sb_y/GaAs$ were prepared using standard mechanical polishing techniques followed by dimpling and low-temperature Ar^+ ion milling. The band alignment of each sample was investigated by using a PHI Quantera SXM XPS system with a monochromated Al Kα (energy of 1486.7 eV) X-ray source with 0.05 eV energy-steps- resolutions. The Ga 3d, O 2s, Al 2p as well as Sb 4d and As 3d CL binding energy spectra and respective valence band maximum were collected with a pass energy of 26 eV and an exit angle of 45°. Both Sb and As CL reference spectra were used to determine the valence band offset as a function of Sb composition, whereby this analysis also provided the error involved in ΔEv. The binding energy was corrected by adjusting the carbon (C) 1s CL peak position to 285.0 eV for each sample surface. Curve fitting was performed by the CasaXPS 2.3.14 using a Lorentzian convolution with a Shirley-type background. The CL energy position was defined to be the center of the peak width at the half of the peak height. The VBM values were determined by linear extrapolation of the leading edge to the baseline of the valence band spectra. The VBM value is sensitive to the choice of points on the leading edge used to obtain the regression line. The uncertainty of ΔE_v values was found to be in the range of ±0.05 eV in the present work by the regressions analysis of selected data over the linear region.

Sample Preparations. All samples were degreased using acetone, isopropanol, and deionized (DI) water. After degreasing, samples were treated under different surface passivation schemes prior to ALD depositions and XPS measurements. The three different surface treatments studied in this work include (1) HCl only, in which the samples were dipped into HCl aqueous solutions for 10 min; (2) $(NH_4)_2S$ only, in which the samples were dipped into 20% $(NH_4)_2S$ aqueous solutions for 10 min; and (3) HCl + $(NH_4)_2S$ treatments, in which the samples were dipped into HCl for 10 min followed by 20% $(NH_4)_2S$ aqueous solutions for another 10 min. A 10 nm (95 cycles and 1.06 Å/cycle) Al_2O_3 layer was deposited at 250 °C using a Cambridge NanoTech ALD system with TMA and DI water as precursors.

AUTHOR INFORMATION

Corresponding Author

*Tel: (540) 231-6663. Fax: (540) 231-3362. E-mail: mantu.hudait@vt.edu.

Notes

The authors declare no competing financial interest.

ACKNOWLEDGMENTS

This work is supported in part by the National Science Foundation (NSF) under grant number ECCS-1348653. J.-S.L. and M.C. acknowledge support from the NSF under grant number ECCS-1348653. The authors would also like to acknowledge the NCFL-Institute for Critical Technology and Applied Sciences (ICTAS) and Virginia Tech Nanofabrication Facilities for materials characterization.

REFERENCES

(1) Delaunay, P.-Y.; Nguyen, B. M.; Hoffman, D.; Huang, E.K.-W.; Razeghi, M. Background Limited Performance of Long Wavelength Infrared Focal Plane Arrays Fabricated from M-Structure InAs−GaSb Superlattices. *IEEE J. Quantum Electron.* **2009**, *45* (2), 157−162.

(2) Boos, J. B.; Kruppa, W.; Bennett, B. R.; Park, D.; Kirchoefer, S. W.; Bass, R.; Dietrich, H. B. AlSb/InAs HEMT's for Low-Voltage, High-speed Applications. *IEEE Trans. Electron Devices* **1998**, *45* (9), 1869−1875.

(3) Bennett, B. R.; Ancona, M. G.; Boos, J. B.; Canedy, C. B.; Khan, S. A. Strained GaSb/AlAsSb Quantum Wells for p-Channel Field-Effect Transistors. *J. Cryst. Growth* **2008**, *311* (1), 47−53.

(4) Zhou, G.; Li, R.; Vasen, T.; Qi, M.; Chae, S.; Lu, Y.; Zhang, Q.; Zhu, H.; Kuo, J. M.; Kosel, T.; Wistey, M.; Fay, P.; Seabaugh, A.; Xing, H. Gate-Recessed Vertical InAs/GaSb TFETs with Record High I_{ON} of 180 μA/μm at V_{DS} = 0.5 V. *IEEE Int. Electron Devices Meet.* **2012**, 777−780.

(5) Datta, S.; Liu, H.; Narayanan, V. Tunnel FET Technology: A Reliability Perspective. *Microelectron. Reliab.* **2014**, *54* (5), 861−874.

(6) Dvorak, M. W.; Bolognesi, C. R.; Pitts, O. J.; Watkins, S. P. 300 GHz InP/GaAsSb/InP Double HBTs with High Current Capability and $BV_{CEO} \geq 6$ V. *IEEE Electron Device Lett.* **2001**, *22* (8), 361−363.

(7) Sun, X.; Wang, S.; Hsu, J. S.; Sidhu, R.; Zheng, X. G.; Li, X.; Campbell, J. C.; Holmes, A. L., Jr. GaAsSb: A Novel Material for Near Infrared Photodetectors on GaAs Substrates. *IEEE J. Sel. Top. Quantum Electron.* **2002**, *8* (4), 817−822.

(8) Qiu, W.; Wang, X.; Chen, P.; Li, N.; Lu, W. Optical Spin Polarization and Hanle Effect in GaAsSb: Temperature Dependence. *Appl. Phys. Lett.* **2014**, *105* (8), 82104.

(9) Blum, O.; Klem, J. F. Characteristics of GaAsSb Single-Quantum-Well-Lasers Emitting near 1.3 μm. *IEEE Photonics Technol. Lett.* **2000**, *12* (7), 771−773.

(10) Anan, T.; Yamada, M.; Nishi, K.; Kurihara, K.; Tokutome, K.; Kamei, A.; Sugou, S. Continuous-Wave Operation of 1.30μm GaAsSb/GaAs VCSELs. *Electron. Lett.* **2001**, *37* (9), 566−567.

(11) Klem, J. F.; Blum, O.; Kurtz, S. R.; Fritz, I. J.; Choquette, K. D. GaAsSb/InGaAs Type-II Quantum Wells for Long-Wavelength Lasers on GaAs Substrates. *J. Vac. Sci. Technol., B: Microelectron. Process. Phenom.* **2000**, *18* (3), 1605−1608.

(12) Kim, Y.; Ban, K. − Y.; Zhang, C.; Honsberg, C. B. Material and Device Characteristics of InAs/GaAsSb Sub-Monolayer Quantum Dot Solar Cells. *Appl. Phys. Lett.* **2015**, *107* (15), 153103.

(13) Eguchi, Y.; Shiokawa, M.; Sakamoto, K.; Yamaguchi, K. Intermediate Band Solar Cells Using In-Plane Ultrahigh-Density InAs/GaAsSb Quantum-Dot Sheets. *IEEE Photovoltaic Spec. Conf.* **2012**, 45−47.

(14) Sun, X.; Hsu, J.; Zheng, X. G.; Campbell, J. C.; Holmes, A. L., Jr. GaAsSb Resonant-Cavity-Enhanced Photodetector Operating at 1.3 μm. *IEEE Photonics Technol. Lett.* **2002**, *14* (5), 681−683.

(15) Sun, X.; Wang, S.; Zheng, X. G.; Li, X.; Campbell, J. C.; Holmes, A. L., Jr. 1.31 μm GaAsSb Resonant-Cavity-Enhanced Separate

DOI: 10.1021/acsami.5b10176
ACS Appl. Mater. Interfaces XXXX, XXX, XXX−XXX

Absorption, Charge and Multiplication Avalanche Photodiodes with Low Noise. *J. Appl. Phys.* **2003**, *93* (1), 774−776.

(16) Liu, J. − S.; Zhu, Y.; Goley, P. S.; Hudait, M. K. Heterointerface Engineering of Broken-Gap InAs/GaSb Multilayer Structures. *ACS Appl. Mater. Interfaces* **2015**, *7* (4), 2512−2517.

(17) Schwartz, G. P. Analysis of Native Oxide Films and Oxide-Substrate Reactions on III−V Semiconductors using Thermochemical Phase Diagrams. *Thin Solid Films* **1983**, *103* (1), 3−16.

(18) Chen, P. T.; Sun, Y.; Kim, E.; McIntyre, P. C.; Tsai, W.; Garner, M.; Pianetta, P.; Nishi, Y.; Chui, C. O. HfO_2 Gate Dielectric on $(NH_4)_2S$ Passivated (100) GaAs Grown by Atomic Layer Deposition. *J. Appl. Phys.* **2008**, *103* (3), 034106.

(19) McDonnell, S.; Zhernokletov, D. M.; Kirk, A. P.; Kim, J.; Wallace, R. M. In Situ X-ray Photoelectron Spectroscopy Characterization of Al_2O_3/GaSb Interface Evolution. *Appl. Surf. Sci.* **2011**, *257* (20), 8747−8751.

(20) Suri, R.; Lichtenwalner, D. J.; Misra, V. Impact of Elemental Arsenic on Electrical Characteristics of Metal-Oxide-Semiconductor Capacitors on GaAs using Atomic-Layer Deposited HfO_2 Gate Dielectric. *Appl. Phys. Lett.* **2008**, *92* (24), 243506.

(21) Misra, D. Issues and Challenges of High-k Dielectrics on High-Mobility Substrates. *ECS Trans.* **2011**, *41* (7), 109−118.

(22) Nainani, A.; Irisawa, T.; Yuan, Z.; Bennett, B. R.; Boos, J. B.; Nishi, Y.; Saraswat, K. C. Optimization of the Al_2O_3/GaSb Interface and a High-Mobility GaSb pMOSFET. *IEEE Trans. Electron Devices* **2011**, *58* (10), 3407−3415.

(23) Barth, M.; Bruce Rayner, G., Jr.; McDonnell, S.; Wallace, R. M.; Bennett, B. R.; Engel-Herbert, R.; Datta, S. High Quality HfO_2/p-GaSb(001) Metal-Oxide-Semiconductor Capacitors with 0.8nm Equivalent Oxide Thickness. *Appl. Phys. Lett.* **2014**, *105* (22), 222103.

(24) Bermudez, V. M. The Effects of The Initial Stages of Native-Oxide Formation on The Surface Properties of GaSb (001). *J. Appl. Phys.* **2013**, *114* (2), 024903.

(25) Hollinger, G.; Skheyta-Kabbani, R.; Gendry, M. Oxides on GaAs and InAs Surfaces: An X-ray-Photoelectron-Spectroscopy Study of Reference Compounds and Thin Oxide Layers. *Phys. Rev. B: Condens. Matter Mater. Phys.* **1994**, *49* (16), 11159−11167.

(26) Ali, A.; Madan, H. S.; Kirk, A. P.; Zhao, D. A.; Mourey, D. A.; Hudait, M. K.; Wallace, R. M.; Jackson, T. N.; Bennett, B. R.; Boos, J. B.; Datta, S. Fermi Level Unpinning of GaSb (100) Using Plasma Enhanced Atomic Layer Deposition of Al_2O_3. *Appl. Phys. Lett.* **2010**, *97* (14), 143502.

(27) Suri, R.; Lichtenwalner, D. J.; Misra, V. Interfacial Self Cleaning During Atomic Layer Deposition and Annealing of HfO_2 Films on Native (100)-GaAs Substrates. *Appl. Phys. Lett.* **2010**, *96* (11), 112905.

(28) Nguyen, N. V.; Kirillov, O. A.; Jiang, W.; Wang, W.; Suehle, J. S.; Ye, P. D.; Xuan, Y.; Goel, N.; Choi, K.-W.; Tsai, W.; Sayan, S. Band Offsets of Atomic-Layer-Deposited Al_2O_3 on GaAs and the Effects of Surface Treatment. *Appl. Phys. Lett.* **2008**, *93* (8), 082105.

(29) Geppert, I.; Eizenberg, M.; Ali, A.; Datta, S. Band Offsets Determination and Interfacial Chemical Properties of The Al_2O_3/GaSb System. *Appl. Phys. Lett.* **2010**, *97* (16), 162109.

(30) Hudait, M. K.; Lin, Y.; Ringel, S. A. Strain Relaxation Properties of $InAs_yP_{1-y}$ Metamorphic Materials Grown on InP Substrates. *J. Appl. Phys.* **2009**, *105* (6), 061643.

(31) Clavel, M.; Goley, P.; Jain, N.; Zhu, Y.; Hudait, M. K. Strain-Engineered Biaxial Tensile Epitaxial Germanium for High-Performance Ge/InGaAs Tunnel Field-Effect Transistors. *IEEE J. Electron Devices Soc.* **2015**, *3* (3), 184−193.

(32) Zhu, Y.; Clavel, M.; Goley, P.; Hudait, M. K. Growth, Strain Relaxation Properties and High-κ Dielectric Integration of Mixed-Anion $GaAs_{1-y}Sb_y$ Metamorphic Materials. *J. Appl. Phys.* **2014**, *116* (13), 134304.

(33) Rajamohanan, B.; Mohata, D.; Zhernokletov, D.; Brennan, B.; Wallace, R. M.; Engel-Herbert, R.; Datta, S. Low-Temperature Atomic-Layer-Deposited High-κ Dielectric for p-Channel $In_{0.7}Ga_{0.3}As$/$GaAs_{0.35}Sb_{0.65}$ Heterojunction Tunneling Field-Effect Transistor. *Appl. Phys. Express* **2013**, *6* (10), 101201.

(34) Hinkle, C. L.; Sonnet, A. M.; Vogel, E. M.; McDonnell, S.; Hughes, G. J.; Milojevic, M.; Lee, B.; Aguirre-Tostado, F. S.; Choi, K. J.; Kim, H. C.; Kim, J.; Wallace, R. M. GaAs Interfacial Self-Cleaning by Atomic Layer Deposition. *Appl. Phys. Lett.* **2008**, *92* (7), 071901.

(35) Zhernokletov, D. M.; Dong, H.; Brennan, B.; Yakimov, M.; Tokranov, V.; Oktyabrsky, S.; Kim, J.; Wallace, R. M. Surface and Interfacial Reaction Study of Half Cycle Atomic Layer Deposited HfO_2 on Chemically Treated GaSb Surfaces. *Appl. Phys. Lett.* **2013**, *102* (13), 131602.

(36) Milojevic, M.; Hinkle, C. L.; Aguirre-Tostado, F. S.; Kim, H. C.; Vogel, E. M.; Kim, J.; Wallace, R. M. Half-Cycle Atomic Layer Deposition Reaction Studies of Al_2O_3 on $(NH_4)_2S$ Passivated GaAs(100) Surfaces. *Appl. Phys. Lett.* **2008**, *93* (25), 252905.

(37) Bard, A. J.; Parsons, R.; Jordan, J. *Standard Potentials in Aqueous Solutions*; Marcel Dekker: New York, 1985.

(38) Kraut, E. A.; Grant, R. W.; Waldrop, J. R.; Kowalczyk, S. P. Semiconductor Core-Level to Valence-Band Maximum Binding-Energy Differences: Precise Determination by X-ray Photoelectron Spectroscopy. *Phys. Rev. B: Condens. Matter Mater. Phys.* **1983**, *28* (4), 1965−1977.

(39) Zhang, F.; Saito, K.; Tanaka, T.; Nishio, M.; Arita, M.; Guo, Q. Wide Bandgap Engineering of $(AlGa)_2O_3$ Films. *Appl. Phys. Lett.* **2014**, *105* (16), 162107.

(40) Huang, M. L.; Chang, Y. C.; Chang, Y. H.; Lin, T. D.; Kwo, J.; Hong, M. Energy-Band Parameters of Atomic Layer Deposited Al_2O_3 and HfO_2 on $In_xGa_{1-x}As$. *Appl. Phys. Lett.* **2009**, *94* (5), 052106.

(41) Wang, T. S.; Tsai, J. T.; Lin, K. I.; Hwang, J. S.; Lin, H. H.; Chou, L. C. Characterization of Band Gap in GaAsSb/GaAs Heterojunction and Band Alignment in GaAsSb/GaAs Multiple Quantum Wells. *Mater. Sci. Eng., B* **2008**, *147* (2), 131−135.

(42) Sze, S. M.; Ng, K. K. *Physics of Semiconductor Devices*, 3rd ed.; John Wiley & Sons: Hoboken, NJ, 2007.

(43) Hudait, M. K.; Zhu, Y.; Goley, P.; Clavel, M.; Jain, N. Mixed-anion GaAs1-ySby Graded Buffer Heterogeneously Integrated on Si by Molecular Beam Epitaxy. *Appl. Phys. Express* **2015**, *8* (2), 025501−025503.

DOI: 10.1021/acsami.5b10176
ACS Appl. Mater. Interfaces XXXX, XXX, XXX−XXX